Journal of Sustainable Development of Energy, Water and Environment Systems

http://www.sdewes.org/jsdewes

Year 2026, Volume 14, Issue 3, 1140702

Original Research Article

Designing for Sustainability: Two-Stage Optimisation of Envelope Efficiency and Photovoltaic–Battery Sizing for a Moroccan Residential Building

Aboubekr Allam*[*1], Bouthayna Slimani[1], Hassan Zahboune[1], Smail Zouggar[1], Mohamed L. Elhafyani[1], Taoufik Ouchbel[1], Nikola Matak[2], Ven Rajlić[2]

[1]University Mohammed 1, School of Technology, Laboratory of Electrical Engineering and Maintenance (LEEM). BP, 473, 60000 Oujda. Morocco

[2]University of Zagreb, Faculty of Mechanical Engineering and Naval Architecture, Ivana Lucica 5, 10000 Zagreb, Croatia

e-mail: bouthayna.slimani.d23@ump.ac.ma, aboubekr.allam@ump.ac.ma, H.zahboune@ump.ac.ma, smail.zouggar@ump.ac.ma, m.elhafyani@ump.ac.ma, t.ouchbel@ump.ac.ma, nikola.matak@fsb.unizg.hr, ven.rajlic@gmail.com

Cite as: Allam, A., Slimani, B., Zahboune, H., Zouggar, S., Elhafyani, M. L., Ouchbel, T., Matak, N., Rajlić, V., Designing for Sustainability: Two-Stage Optimisation of Envelope Efficiency and Photovoltaic–Battery Sizing for a Moroccan Residential Building., J.sustain. dev. energy water environ. syst., 14(3), 1140702, 2026,
DOI: https://doi.org/10.13044/j.sdewes.d14.0702

ABSTRACT

Moroccan buildings remain electricity-intensive despite ambitious renewable-electricity targets, and household energy economics are shaped by tariff design and export limitations. This study develops a two-stage optimisation framework that couples genetic-algorithm envelope optimisation (DesignBuilder/EnergyPlus) with a dispatch-constrained mixed-integer linear programme that co-optimises rooftop photovoltaic and battery capacities and hourly operation over 8,760 h under Morocco's time-of-use tariff, a no-grid-to-battery charging rule, and export constraints. For a representative dwelling in Oujda, envelope upgrades reduce annual space-conditioning electricity demand by 26.9%. Under self-consumption with unpaid exports, the cost-optimal design shifts from 8.0 kW photovoltaic without storage (self-supply ratio 46.4%) to 10.4 kW photovoltaic with 11.8 kWh storage (self-supply ratio 76.6%), reducing annual total cost by 18.6%. When paid exports are enabled under a 20% annual quota, the optimum becomes 10.9 kW photovoltaic with 13.5 kWh storage (self-supply ratio 81.3%) and annual total cost decreases by 9.8% through surplus value recovery. Capacity sweeps confirm diminishing marginal returns: beyond the optima, additional capacity increasingly converts into curtailment or low-value surplus, increasing annual total cost and the levelized cost of electricity. A policy grid over export remuneration and permitted export share identifies a regime transition at a 70% export allowance, beyond which photovoltaic capacity reaches a stable plateau and optimal storage requirements decrease as the economic driver shifts from time shifting toward direct surplus sales. The results support an efficiency-first, then optimal-sized photovoltaic-plus-storage strategy and highlight the importance of bankable export remuneration and broader time-of-use participation for improving household economics.

KEYWORDS

Renewable integration, BIM, Photovoltaic systems, Energy efficiency, Cost optimization, Mixed-integer linear programming.

INTRODUCTION

Morocco has set ambitious targets for renewable electricity, aiming to supply over half of its power from renewable sources by 2030 [1]. At the same time, the building sector

(residential and tertiary) remains a major driver of energy demand, reported at 32% of national final energy consumption, which makes demand-side efficiency a central lever for meeting these transition objectives [2]. Morocco also benefits from strong solar potential: annual global horizontal irradiance commonly falls in the 5 – 6 kWh/m^{2}day range across much of the country [3], positioning rooftop photovoltaic (PV) systems as a credible option to reduce grid dependence and enhance household energy resilience. Realising this potential in the residential sector, however, typically requires PV deployment to be coordinated with envelope-level efficiency improvements and storage, so that generation is better aligned with household load patterns and local market rules.

Recent Morocco-specific transmission analyses further show that higher renewable penetration can significantly reshape power flows and reveal bottlenecks, reinforcing the value of coordinated distributed PV and flexibility resources [4]. Residential PV adoption is therefore shaped not only by technology costs, but also by retail pricing and prosumer regulations. The national utility (ONEE) offers an optional time-of-use (TOU) tariff for eligible low-voltage consumers, introducing a price signal that can increase the value of storage by shifting PV-derived electricity from daytime production toward higher-value evening periods [5]. Recent studies further indicate that the economic value of residential batteries depends strongly on tariff structure, export compensation, and dispatch strategy under time-varying prices [6]. More broadly, scenario-based policy analyses show that incentive design and market rules can materially change system feasibility and the distribution of benefits across configurations, which motivates treating tariff and export assumptions explicitly in optimization [7]. In parallel, PV economics depends strongly on how surplus exports are treated and on the operating conditions that apply to residential storage within the self-production framework. The regulatory environment further complicates PV economics. ANRE Decision No. 04/26 sets the tariff for surplus electrical energy produced under Laws No. 40-19 and No. 82-21, while surplus sales remain limited to 20% of annual production [8]. Implementing decrees were still being drafted at the time of the latest ANRE report, and no standard feed-in tariff has been promulgated for the low-voltage residential case. As a result, households effectively operate under a self-consumption paradigm: exported energy is either curtailed or accepted by the grid without remuneration. In addition, Morocco prohibits charging residential batteries from the grid. These constraints partial TOU participation, capped surplus sales, and no grid-to-battery charging necessitate design methods that maximise self-consumption while respecting regulatory limits.

Building-energy research in North Africa has progressed along two largely independent trajectories: building-envelope optimisation and PV – battery system optimisation. In the first trajectory, meta-heuristic approaches are widely used to explore interacting passive measures and their combined impact on end-use demand. De Oliveira *et al.* report that retrofit strategies to improve building energy efficiency and sustainability commonly combine envelope insulation, improvements to climatisation and lighting systems, and the integration of renewable energy sources, with the preferred measures varying according to climate and building characteristics [9]. In Morocco, Abdou *et al.* apply multi-objective optimisation of passive energy-efficiency measures for net-zero energy building design, explicitly balancing demand reduction and performance trade-offs within dynamic simulation [10]. Recent Moroccan studies extend this line of work using climate-zone-specific modelling and multi-objective formulations: Boumlik *et al.* optimise insulation and glazing across six Moroccan climate zones and discuss pathways toward near/net-zero performance in residential buildings [11], while Benaddi *et al.* couple TRNSYS with GenOpt to identify envelope solutions that balance economic, environmental, and thermal-comfort criteria across the same climatic diversity [12]. More broadly, recent systematic evidence indicates that GA-based multi-objective retrofit optimisation is becoming increasingly sophisticated, particularly through the continued dominance of NSGA-II and the growing integration of life-cycle analysis and dynamic simulation tools [13]. Nevertheless, this envelope-optimisation stream is

rarely coupled to PV – battery sizing and dispatch under time-varying retail prices and prosumer constraints, even though storage value is inherently time-dependent.

The second trajectory focuses on PV–battery sizing and dispatch, most commonly formulated as mixed-integer linear programming (MILP). Early tariff-aware work by Jakus *et al.* showed that jointly optimising PV and battery capacities with coordinated scheduling across alternative retail tariff structures can deliver substantial bill reductions, particularly under net billing and dynamic pricing [14]. Subsequent residential studies showed that battery economics are highly sensitive to electricity price variability, whereas well-sized PV-only systems remained the more financially robust option under varying electricity-price conditions [15]. Recent building-focused studies further treat PV – battery sizing as a constraint-aware optimisation problem using time-resolved demand: Yu *et al.* optimise PV-battery configurations for existing buildings under transformer-capacity constraints, while a recent Buildings study applies NSGA-II to size PV-battery systems for detached houses using hourly load profiles and testing robustness under different electricity-price conditions [16], [17]. More recent contributions have strengthened modelling realism by incorporating behind-the-meter uncertainty and degradation-aware cycling limits in the sizing problem [18], and by extending MILP-based home energy management models to represent battery cycle degradation more explicitly, including the influence of operating patterns on battery degradation [19]. In parallel, Moroccan studies have begun to provide locally grounded evidence on residential energy performance and management under national conditions, including the effects of climate-dependent construction practices and thermal-regulation compliance [20], together with forecast-based, tariff-aware optimisation of PV – battery operation in residential smart microgrids under the Moroccan pricing framework [21]. Recent work further shows that day-ahead MILP-based battery scheduling can improve economic outcomes while preserving grid stability when forecasted PV generation, tariff structures, and voltage constraints are incorporated explicitly into the optimisation framework [22]. Beyond single dwellings, recent studies on multi-story and community-scale settings show that coordinated or shared storage can improve solar utilisation, reduce grid dependence, and strengthen the economic value of collective self-consumption [23], [24]. Complementary optimisation-driven work also shows that energy-flow scheduling can materially improve performance indicators in PV-based systems; for instance, Dadjiogou *et al.* demonstrate PSO-based energy-flow management for a PV microgrid supplying multiple loads [25].

Despite these advances, most PV – battery optimisation studies still treat building demand as an exogenous input and rarely couple envelope-driven load changes with prosumer-policy constraints and operationally feasible battery dispatch, leaving the synergy between passive demand reduction and cost-optimal PV – battery design insufficiently explored.

A further limitation in the PV – battery literature is that "optimisation" is sometimes used loosely: several studies effectively compare a small set of predefined scenarios, while others employ simplified formulations that can produce dispatch patterns that are not operationally feasible. More broadly, this reinforces a key need in residential prosumer studies: PV – battery sizing should be assessed with (i) realistic, time-resolved building demand and (ii) policy- and tariff-consistent operational constraints, because storage value is fundamentally time-dependent.

To address these gaps, this paper proposes a coupled workflow in which a GA-based envelope optimisation generates an hourly demand profile that feeds a policy-consistent MILP for PV – battery sizing and dispatch under time-varying retail prices and prosumer export rules. The framework is designed to produce operationally valid schedules and to represent key policy levers that shape household economics. Using this setup, the analysis quantifies where additional PV or storage yields diminishing marginal benefit and assesses how alternative export-remuneration assumptions shift the cost-optimal design relative to a self-consumption baseline. By integrating envelope optimisation with dispatch-constrained PV–battery optimisation, the resulting capacity choices can differ materially from approaches that treat demand reduction and supply sizing as separate problems.

METHOD

A two-stage optimisation framework is developed to produce operationally credible and policy-compliant photovoltaic–battery designs by coupling envelope-driven demand reduction with mixed-integer linear programming dispatch and sizing. First, a multi-objective genetic algorithm (GA) implemented in DesignBuilder with the EnergyPlus simulation engine explores feasible combinations of insulation and glazing for a representative dwelling in Oujda. The optimisation seeks to reduce annual electricity demand for heating and cooling while respecting thermal comfort constraints and limiting additional construction cost. This stage produces an hourly electricity load profile for a full year (8,760 hours). Second, a mixed-integer linear programming (MILP) model selects the photovoltaic capacity and the battery capacity and optimises hourly energy routing between photovoltaic generation, the battery, and the grid under Morocco's time-of-use tariff and the assumed export conditions. Battery operation is represented using state-of-charge dynamics with a cyclic boundary condition, charging and discharging efficiency losses, and mutually exclusive operating modes enforced through binary variables with a big-M formulation linked to the battery power limit. Policy switches represent alternative regulatory settings, including disabling grid-to-battery charging and changing export remuneration assumptions. A post-optimisation capacity-perturbation analysis is then applied by incrementally increasing photovoltaic and battery sizes and re-optimising dispatch for each case. This analysis is used to identify cost – performance plateaus and quantify the sensitivity of optimal designs to export and tariff settings.

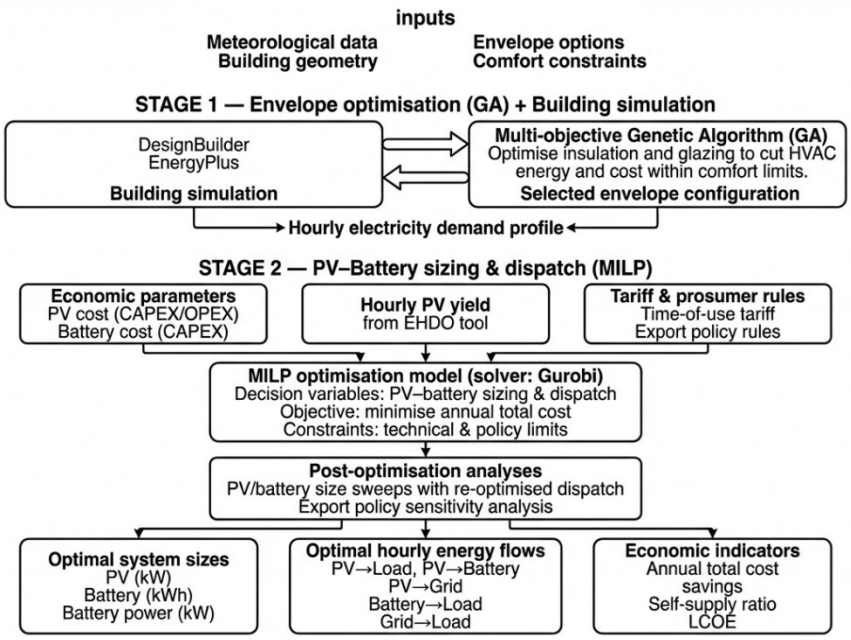

Figure 1. Overview of the approach

Figure 1 illustrates the general methodological framework adopted in this study, integrating building energy simulation, envelope optimization using GA, and renewable energy system optimization via MILP.

Building Energy Simulation

Detailed hourly energy consumption profiles were generated using DesignBuilder software, which interfaces directly with EnergyPlus simulation engine [26]. Hourly data for a full year (8,760 hours) were simulated based on critical input parameters:

- Local climatic data (hourly solar radiation, ambient temperature, wind speed).

- Defined building geometry, including spatial layout and orientation.
- Thermal and physical properties of construction materials (insulation, glazing, wall, roof, floor layers).
- Internal zoning and Heating, ventilation, and air conditioning HVAC system specifications.

Envelope Optimization using Genetic Algorithm

Envelope performance optimization was performed utilizing GA integrated within the DesignBuilder simulation environment. The GA systematically evaluated numerous envelope configurations considering insulation types and thicknesses, glazing specifications, and roof insulation strategies.

Optimization targeted the minimization of annual HVAC energy demands and incremental construction costs. A multi-objective optimization approach was employed, resulting in a set of Pareto-optimal envelope configurations. The fitness function simultaneously minimized:

- Annual HVAC energy demand (operational cost).
- Incremental construction costs (economic viability).

Envelope configurations considered in the GA optimization process included various commercially available insulation materials and glazing systems specifically selected for relevance to regional market availability.

Photovoltaic and Battery Mixed-Integer Linear Program

A grid-connected residential PV – battery system is co-optimised over a one-year horizon, Decision variables include PV power P_{pv} (kW) and BESS energy C_{bat} (kWh), with power capability implied by the C_{rate}(kW/kWh). Hourly dispatch variables route energy among the load, the battery and the grid. Exogenous inputs are hourly electric demand L^t (kWh), specific PV yield PV^t (kWh/kW), and grid import price p^t (USD/kWh). Hourly PV potential PV^t is generated using the open-source Energy Hub Design Optimization (EHDO) solar modelling approach, yielding a physically consistent kWh/kW profile that directly enters the PV resource constraint [27], [28].

Objective function: The objective minimises the annual total cost as the sum of (i) hourly operating terms grid import payments and PV variable O&M, plus a reliability penalty for any unserved load net of (ii) export revenues, and (iii) capital costs annualised via the capital recovery factor (CRF):

$$\begin{aligned}&\text{Min } \sum_{t=1}^{8760}\left[P^t\left(E^t_{\mathrm{g}\to\mathrm{l}}+E^t_{\mathrm{g}\to\mathrm{b}}\right)+C_{\mathrm{pv,OM}}\left(E^t_{\mathrm{p}\to\mathrm{l}}+E^t_{\mathrm{p}\to\mathrm{b}}+E^t_{\mathrm{p}\to\mathrm{g}}\right)+c_{\mathrm{LL}}\times LL^t\right]+\\&\mathrm{CRF}\left(c_{\mathrm{pv}}\times P_{\mathrm{pv}}+c_{\mathrm{bat,E}}\times C_{\mathrm{bat}}+c_{\mathrm{bat,P}}\times C_{\mathrm{rate}}\times C_{\mathrm{bat}}\right)-\sum_{t=1}^{8760}P_{\mathrm{exp}}\times E^t_{\mathrm{p}\to\mathrm{g}}\end{aligned}\qquad(1)$$

The objective minimises the annual total system cost eq. (1), aggregating operating payments and penalties, export revenues, and annualised investments; its constituent terms are:

- Grid electricity cost Operating payments for grid energy delivered to the load $E^t_{\mathrm{p}\to\mathrm{l}}$ and where policy permits to charge the battery $E^t_{\mathrm{g}\to\mathrm{l}}$.
- PV variable $C_{\mathrm{pv,OM}}$. A marginal per-kWh operating charge applied to all PV generation, regardless of its sink (self-consumption, storage, export).
- Reliability (lost-load) penalty. A high shadow cost on unserved energy LL^tthat approximates the Value of Lost Load. With a sufficiently large c_{LL}, infeasible or policy-induced shortages are the only circumstances under which LL^t>0.
- Export revenue. Credits remunerated PV exports at the applicable price. Policy instruments (annual export quota) do not alter this revenue term but constrain $E^t_{\mathrm{p}\to\mathrm{g}}$ (eq. (17)), thereby capping total export earnings.

- Annualised investment cost (CAPEX). Capital charges are annualised using the CRF and applied separately to each component: PV capacity, battery energy capacity, and battery power capacity. The PV cost is proportional to the installed PV power, the battery pack cost is proportional to its usable energy (kWh), and the battery interface cost scales with the implied power ($C_{\text{rate}} \times C_{\text{bat}}$), reflecting inverter-related expenditures.

Constraints. The formulation is further bounded by constraints eq. (2) to eq. (18), which together impose hourly energy conservation at the load, govern battery state-of-charge (*SOC*) dynamics within admissible limits, restrict charge/discharge magnitudes to the inverter rating through tight big-M gating, prevent physically inconsistent simultaneous charge – discharge, encode policy switches such as bans on grid-to-battery charging, and allocate PV energy derived from EHDO-specific yields across self-consumption, storage, and export. The starting point is the hourly balance at the point of consumption, as in eq. (2), which requires that the demand be met by local PV, battery discharge, or the grid, with any shortfall recorded as lost load; in this identity, the left-hand side aggregates deliveries to the load, while $LL^t \geq 0$ captures unmet demand and is penalised in the objective function eq. (1), ensuring that reliability impacts are explicitly costed in eq. (2):

$$E^t_{\text{p}\to\text{l}} + E^t_{\text{b}\to\text{l}} + E^t_{\text{g}\to\text{l}} + LL^t = L^t \quad \forall t \tag{2}$$

Battery energy evolves over time with one-way efficiencies, the initial *SOC* is set as a fraction of installed capacity, a cyclic terminal condition avoids end-effects, and a usable band preserves both operability and longevity, eq. (3) to eq. (6). Specifically, eq. (3) advances *SOC* by accounting for charged energy from PV and (when permitted) the grid, and for delivered discharge after efficiency losses; eq. (4) and eq. (5) enforce a closed annual cycle; and eq. (6) restricts operation to the admissible *SOC* range:

$$SOC^t = SOC^{t-1} + \eta_{\text{chg}}\left(E^t_{\text{p}\to\text{b}} + E^t_{\text{g}\to\text{b}}\right) - \frac{1}{\eta_{\text{dis}}} E^t_{\text{b}\to\text{l}} \quad \forall t \tag{3}$$

$$SOC^1 = SOC^0\, C_{\text{bat}} \tag{4}$$

$$SOC^1 = SOC^{8760} \tag{5}$$

$$SOC_{\text{min}}\, C_{\text{bat}} \leq SOC_t \leq C_{\text{bat}} \quad \forall t \tag{6}$$

Per-hour charge and discharge magnitudes are bounded by the battery's rated power $C_{\text{rate}} \times C_{\text{bat}}$; binary mode variables gate the active operation with a big-M equal to that physical limit, yielding a tight relaxation and precluding spurious fractional activity eq. (7) to eq.(11) with eq. (7) and eq. (8) imposing aggregate power bounds and eq. (9) to eq. (11) ensuring that only the flagged mode can carry energy in a given hour:

$$\mathrm{E}^{\mathrm{t}}_{\mathrm{b}\to\mathrm{l}} \leq \mathrm{C}_{\mathrm{rate}}\, \mathrm{C}_{\mathrm{bat}} \quad \forall \mathrm{t} \tag{7}$$

$$\mathrm{E}^{\mathrm{t}}_{\mathrm{p}\to\mathrm{b}} + \mathrm{E}^{\mathrm{t}}_{\mathrm{g}\to\mathrm{b}} \leq \mathrm{C}_{\mathrm{rate}}\, \mathrm{C}_{\mathrm{bat}} \quad \forall \mathrm{t} \tag{8}$$

$$\mathrm{E}^{\mathrm{t}}_{\mathrm{p}\to\mathrm{b}} \leq \mathrm{C}_{\mathrm{rate}}\, \mathrm{C}_{\mathrm{bat}}\, \mathrm{y}^{\mathrm{t}}_{\mathrm{chg,pv}} \quad \forall \mathrm{t} \tag{9}$$

$$\mathrm{E}^{\mathrm{t}}_{\mathrm{g}\to\mathrm{b}} \leq \mathrm{C}_{\mathrm{rate}}\, \mathrm{C}_{\mathrm{bat}}\, \mathrm{y}^{\mathrm{t}}_{\mathrm{chg,grid}} \quad \forall \mathrm{t} \tag{10}$$

$$E^{t}_{b\to l} \le C_{rate}\, C_{bat}\, y^{t}_{dis} \quad \forall t \tag{11}$$

These limits ensure that instantaneous flows never exceed the rated interface and that only the flagged mode can carry energy in a given hour.

Exclusivity at the hourly timescale rules out simultaneous charging and thereby simplifying feasible operating patterns and removing physically inconsistent behaviours from the solution space; this is enforced by constraints eq. (12) and eq. (13):

$$y^{t}_{chg,pv} + y^{t}_{dis} \le 1, \quad \forall t \tag{12}$$

$$y^{t}_{chg,grid} + y^{t}_{dis} \le 1 \quad \forall t \tag{13}$$

Jurisdictions in which batteries may not be charged from the grid are represented by shutting the corresponding flow and mode eq. (14); the switch eliminates import-arbitrage and forces the battery to operate as a buffer for PV surplus only:

$$E^{t}_{g\to b} = 0, y^{t}_{chg,grid} = 0 \quad \forall t \tag{14}$$

Hourly PV energy is bounded by the resource available from the installed array and is allocated across direct self-consumption, charging, and export eq. (15) and eq. (16); here PV^{t} is the EHDO-derived specific yield (kWh/kW) and scales linearly with P_{pv}, thereby preserving the underlying irradiance and temperature physics:

$$E^{t}_{p\to l} + E^{t}_{p\to b} + E^{t}_{p\to g} \le PV^{t}_{resource} \quad \forall t \tag{15}$$

$$PV^{t}_{resource} = P_{pv} \times PV^{t} \quad \forall t \tag{16}$$

In paid-export scenarios, annual PV exports are capped as a fraction of total PV production. To keep the optimisation linear, this is reformulated in eq. (17). The 20% export quota is implemented by an equivalent identity: exported PV energy must be less than or equal to 20% of total PV generation (that is, the sum of direct PV to load, PV to battery, and PV to grid). Rearranging gives an equivalent condition: exported PV must be less than or equal to 25% of the sum of PV to load and PV to battery. This transformation ensures that the quota is respected while preserving the MILP structure, effectively limiting total export revenues in line with policy:

$$\sum_{t=1}^{8760} E^{t}_{p\to g} \le 0.25 \sum_{t=1}^{8760} \left(E^{t}_{p\to l} + E^{t}_{p\to b}\right) \tag{17}$$

Case Study Description

The case study involves a two-story, single-family urban residential building located in Oujda, within Morocco's Oriental region (climatic Zone 3), as shown in **Figure 3**. The building exhibits a typical compact Moroccan residential architecture with a central courtyard designed for daylighting and natural ventilation [2]. It covers approximately 114 m², with the ground floor consisting of a garage, kitchen, reception area, hall, and living room, while the upper floor accommodates bedrooms, a lounge, and bathroom facilities **Figure 2**.

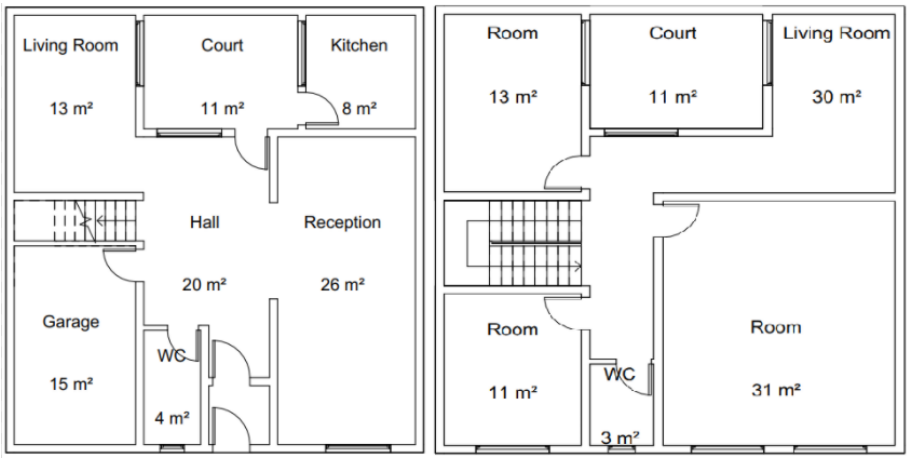

Figure 2. Ground floor and first-floor layouts of the case study building

Climate data for Oujda was sourced from the Meteonorm database (Oujda-Angads station, 34.787°N, – 1.924°E, elevation 467.9 m) [29], [30]. The climate characteristics include:

- Peak summer temperatures frequently exceeding 38 °C.
- Annual mean temperatures ranging between 17.5 and 19.2 °C.
- Low annual precipitation (<350 mm/year).

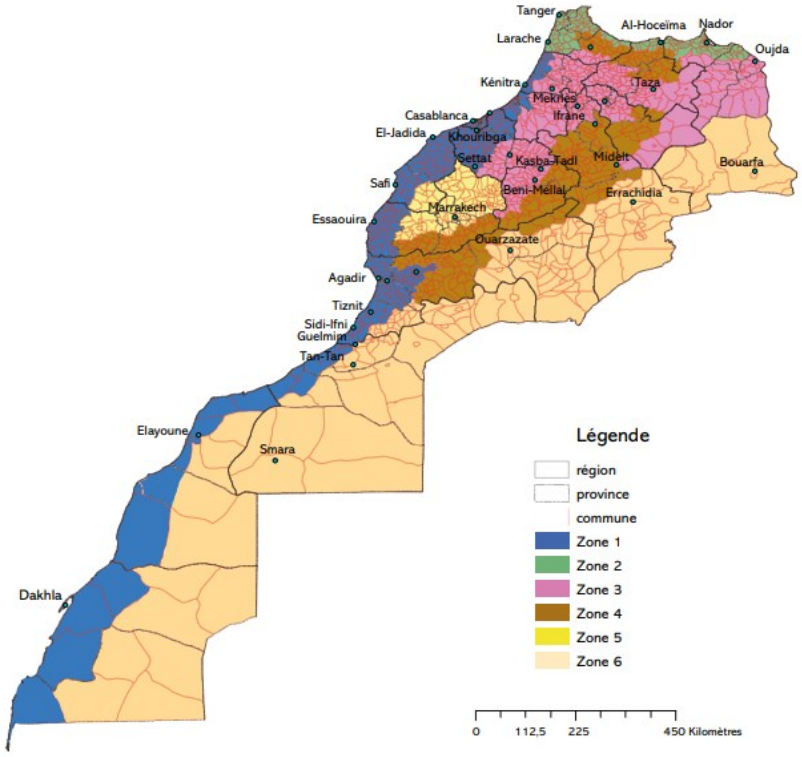

Figure 3. Morocco climatic zones, indicating the study area within Zone 3 [2]

Simulation Parameters

Using DesignBuilder interfaced with EnergyPlus, comprehensive building simulations were performed. Essential simulation parameters included detailed specifications of building envelope elements (walls, roofs, windows, floors), thermal properties such as thermal conductivity, density, and specific heat capacity, and hourly analysis to capture thermal load variations throughout the year. The operational settings considered were a heating setpoint of 20 °C, a cooling setpoint of 26 °C.

Space conditioning in the case-study dwelling is represented by an air-to-air electric heat pump system modelled in DesignBuilder using the Detailed HVAC option. The system is parameterised with an autosized nominal capacity and a single constant efficiency characterised by a coefficient of performance *COP* = 3.2 (Wh/Wh), defined as the ratio between thermal output delivered to the dwelling and the corresponding electrical energy input to the heat-pump system [31]. This *COP* value is held constant across all simulation and optimisation cases. In the analysis, the performance of the system is evaluated exclusively in terms of final energy use.

Envelope Components: The simulation model incorporated detailed envelope component properties [32], summarized in the **Table 1**.

Table 1. Thermal Properties of Building Envelope Components

Component	Material Layer	Thickness (cm)	Thermal Conductivity (W/mK)	Density (kg/m³)	Thermal Capacity (kJ/kgK)
Exterior Wall	Cement Plaster	2	1.153	1700	1.00
	Hollow Brick	2	0.501	720	0.794
	Polystyrene (Insulation)	2–18	0.0392	25	1.38
	Hollow Brick	2	0.501	720	0.794
	Cement Plaster	2	1.153	1700	1.00
Roof	Cement Plaster	2	1.153	1700	1.00
	Concrete Block	16	1.090	1300	0.65
	Concrete (Top Layer)	4	1.755	2300	0.92
	Cement Plaster	2	1.153	1700	1.00
Interior Wall	Hollow Brick	2	0.501	720	0.794
	Cement Plaster	2	1.153	1700	1.00
Windows	Material	Thickness (mm)	U-Value (W/m²K)		
	Single clear	2.5	5.74		

Table 2. summarizes the insulation and glazing materials considered during the optimization, including their specific thermal characteristics and associated costs [31]. Envelope Optimization Measures and Costs

Energy Efficiency Measure (EEM)	Option Description	Cost (USD/m²)
Window Glazing U (W/m²K), Material, thickness(mm)	U = 2.95 W/m²K, Double glazing (air), 2.5/12.7/2.5 mm	90
	U = 1.76 W/m²K, Double glazing + Low-E, 3/12.7/2.5 mm	102
	U = 0.7 W/m²K, Triple glazing + Low-E + Argon, 4/16/4/16/4 mm	130
Wall Construction R (m²K/ W), Material, thickness	R = 1, Polystyrene, 3 cm	68.46
	R = 2, Polystyrene, 6 cm	71.05

Energy Efficiency Measure (EEM)	Option Description	Cost (USD/m²)
(cm)	R = 3, Glass wool, 6 cm	74.41
	R = 4, Phenolic foam, 6 cm	77.51
	R = 5, SIP, 5 cm	82.88
	R = 6, ICF, 6 cm	90.88
Roof Construction R (m²K/W), Material, thickness (cm)	R = 1, Polystyrene, 3 cm	114.95
	R = 2, Polystyrene, 6 cm	117.53
	R = 3, Glass wool, 6 cm	120.89
	R = 4, Phenolic foam, 7 cm	124.70
	R = 5, SIP, 6 cm	132.07
	R = 6, ICF, 6 cm	140.07

Hourly electricity demand for the Oujda dwelling is taken from the building simulation as the series L^t over one year; the site-specific PV yield PV^t for the same period is generated consistently with the Methodology and enters the PV resource constraint, eq. (16) to eq. (17). Together with the study-year tariffs p^t (import), $p^t_{\text{exp}}(export, when\ applicable)$, these time series are supplied to the MILP, which co-determines PV and BESS capacities and hourly dispatch by minimising the annual objective in eq. (1) subject to the operational and policy constraints eq. (2) to eq. (18).

To estimate site PV generation P_{pv}, the open-source EHDO modeling chain was used to produce hourly AC PV yield from the same EPW weather file employed in the DesignBuilder simulations, ensuring meteorological consistency. The setup used the project coordinates (34.68° N), south-facing modules at 30° tilt, nominal module efficiency 18%, and a combined loss derate of 14% (soiling, mismatch, wiring, availability). EHDO applies plane-of-array transposition, incidence-angle and temperature corrections, and DC-to-AC conversion via an inverter-efficiency treatment; accordingly, the PV time series supplied to the MILP is already inverter-inclusive on the AC side. Further modeling details are documented in the EHDO reference **[33]**.

The PV-battery system's economic viability is evaluated under Morocco's time-of-use (TOU) electricity tariff structure set by the National Office of Electricity and Drinking Water (ONEE)**[5]**, which distinguishes between Peak Hours (PH) and Normal Hours (NH) with seasonal variation: in winter (October – March), PH are 17:00 – 22:00 and NH are 22:00 – 17:00; in summer (April –September), PH are 18:00 – 23:00 and NH are 23:00 – 18:00. Corresponding electricity prices are 0.226 USD/kWh during PH and 0.125 USD/kWh during NH, incentivizing load shifting and battery storage utilization to reduce costs. The MILP optimization model incorporates key economic parameters, including a PV installation cost of 1,208 USD/kW, battery cost of 604 USD/kWh, PV operational cost of 0.020 USD/kWh, battery round-trip efficiency of 81%, a project lifespan of 25 years, and a discount rate of 3%, enabling a comprehensive evaluation of the system's lifecycle performance. The MILP uses the PV and battery techno-economic parameters reported in **Table 3**, including PV investment and operating costs, battery energy and power investment costs, the implied power-to-energy ratio C_{rate}, charge and discharge efficiencies, and the economic assumptions (investment horizon and discount rate).

Table 3. Techno-economic input parameters for the photovoltaic (PV) and battery energy storage system

Component	Parameter	Unit	Value
PV	PV_CAPEX	USD/kW	865.0
	CPVOM	USD/kWh/y	20.0
Battery	BAT_CAPEX_ENERGY	USD/kWh	203.0
	BAT_CAPEX_POWER	USD/kW	812.0
	C_{rate}	–	0.5
	EFF_CHAR	–	0.98
	EFF_DIS	–	0.98
Economics	INVEST_YEARS	y	25
	DISC_RATE	–	0.03

To structure the analysis and isolate policy effects, the same core formulation is evaluated under three scenarios:

S1: PV-only. Battery capacity is fixed to zero ($C_{\mathrm{bat}} = 0$ kWh); exports are unpaid ($p^{\mathrm{t}}_{\mathrm{exp}} = 0\mathrm{USD/kWh}$), so the export-quota constraint eq. (17) is inactive. Only PV capacity and dispatch are optimised under eq. (2) to eq. (16), reflecting pure self-consumption with temporal mismatch between midday PV and evening demand.

S2: PV+BESS. PV and BESS capacities are co-optimised; charging from the grid is disabled via the policy switch eq. (15) ($E^{t}_{\mathrm{g\to b}} = 0$ kWh, $y^{t}_{\mathrm{chg,\,grid}} = 0$). Exports remain unpaid ($p^{t}_{\mathrm{exp}} = 0$ USD/kWh). Constraints, eq. (2) to eq. (17) govern dispatch, so storage buffers only PV surplus, enabling time-shifting but not price arbitrage.

S3: PV+BESS with paid export (20% quota). The no-grid-charge policy (14) remains in force; exports are remunerated as specified in the Methods, and the annual export quota is activated via eq. (17). PV and BESS are co-optimised with dispatch governed by eq. (2) to eq. (17), allowing monetisation of residual PV once the load and battery charging requirements have been met.

With these inputs, a single MILP simultaneously determines the optimal PV and battery capacities ($P^{*}_{\mathrm{pv}}, C^{*}_{\mathrm{bat}}$) and the associated hourly dispatch over the study year by minimising the annual objective (1) subject to the operational and policy constraints eq. (2) to eq. (17), thereby producing hourly energy flows and the aggregated performance indicators for the year. Sensitivity analysis is then conducted by evaluating a discrete grid of capacity pairs in the neighbourhood of ($P^{*}_{\mathrm{pv}}, C^{*}_{\mathrm{bat}}$) PV capacity (kW) and battery energy capacity (kWh) are perturbed in predefined increments, capacities are treated as fixed parameters, and the MILP is re-solved under the same constraints eq. (2) to eq. (18) to obtain the corresponding dispatch and recompute the annual total cost as operating terms (net of revenues) plus annualised capital costs, consistent with eq. (1). One-dimensional slices (varying P_{pv} at C^{*}_{bat} , and varying C_{bat} at P^{*}_{pv},) are also examined to isolate marginal effects. The sweeps in any direction is terminated when additional capacity becomes non-profitable, i.e., when an incremental step fails to reduce the objective or increases the annual total cost after accounting for annualised investment and operating terms, and it is truncated when binding policy or technical limits (e.g., the export quota) prevent further changes in dispatch. This procedure yields a local response surface for cost and performance metrics, identifies binding constraints, and quantifies the robustness of the optimal sizing.

To assess the robustness of the paid-export design under alternative policy settings, the full-year MILP was re-solved on a two-dimensional grid of export remuneration p_{exp} and permitted annual export share S_{exp}.

For each combination $(p_{\mathrm{exp}}, S_{\mathrm{exp}})$ the optimisation jointly determines the investment decisions (P_{pv},C_{bat}) and the corresponding hourly dispatch over 8,760 h, while retaining the same operational structure and feasibility constraints as the paid-export case. In this sensitivity formulation, grid-to-battery charging is enabled, allowing the battery to charge from the grid. The export quota is enforced by replacing the fixed-share from eq. (17) whit the eq. (18):

$$\sum_{t=1}^{8760} E_{\mathrm{p\to g}}^{t} \leq \frac{S_{\mathrm{exp}}}{1-S_{\mathrm{exp}}} \sum_{t=1}^{8760} \left(E_{\mathrm{p\to l}}^{t} + E_{\mathrm{p\to b}}^{t}\right) \tag{18}$$

RESULT AND DISCUSSION

The baseline energy simulation indicated an Energy Use Intensity (*EUI*) of approximately 115.84 kWh/m²/year, consistent with regional benchmarks [2], [34]. The monthly electricity demand for heating and cooling, Figure 4 show that space heating is concentrated in the winter months (December – February), while cooling dominates during the summer (June – September), with peak demand in July and August. This seasonal pattern reflects the climatic conditions of Oujda and the thermal characteristics of the uninsulated building.

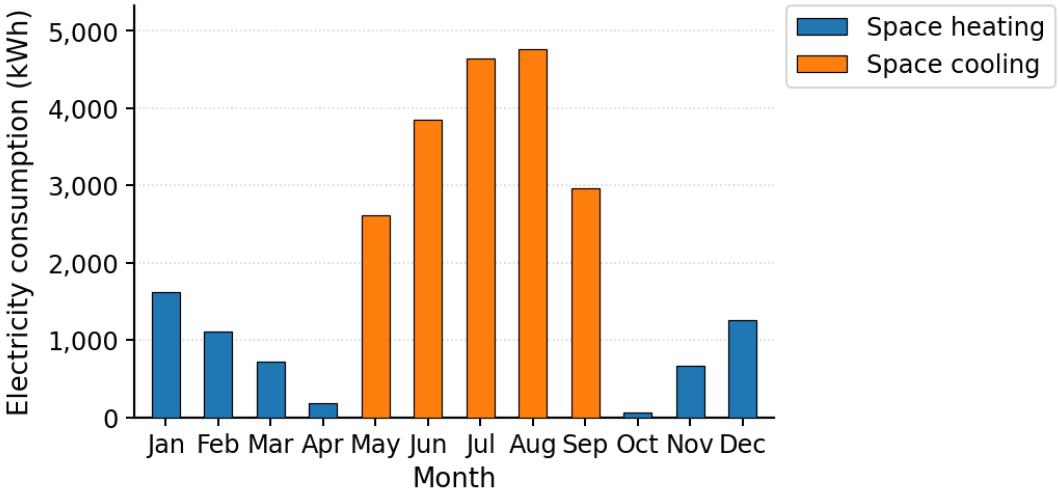

Figure 4. Monthly Heating and Cooling Electricity Demand for the Uninsulated Building

Envelope Optimization

Envelope optimisation was performed using a multi-objective GA to explore insulation and glazing alternatives and identify robust trade-offs between annual HVAC electricity consumption and incremental construction costs. In total, 245 envelope configurations were evaluated Figure 5, producing a Pareto set from which a compromise solution was selected for subsequent PV – battery optimisation. The selected envelope consists of 3 cm polystyrene insulation applied across the envelope elements considered in the optimisation and double glazing filled with air (U=2.95 W/m²K).

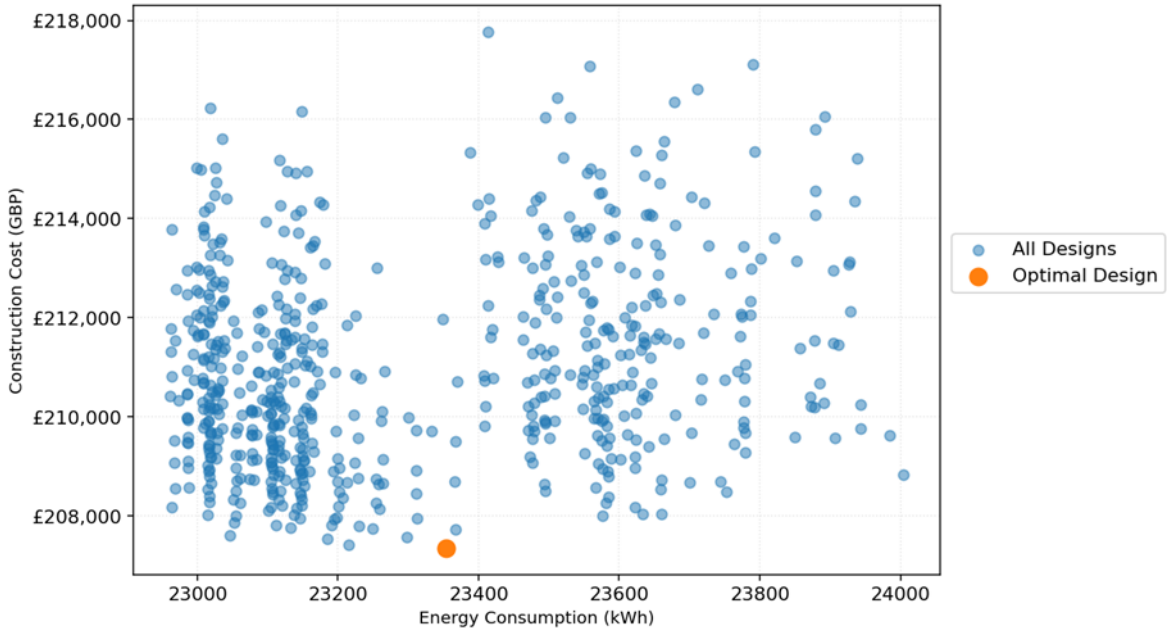

Figure 5. Energy Consumption and Construction Cost – GA Optimization Results

The selected envelope reduces annual HVAC electricity consumption by 26.9% relative to the uninsulated baseline **Figure 6**. The reduction is most pronounced during winter (December – February), reflecting lower transmission losses, while a modest increase in cooling electricity may appear during the warm season (May – September). This trade-off is consistent with the "anti-insulation" effect reported for warm and semi-arid climates when night ventilation and external shading are not enabled, as increased thermal resistance can limit nocturnal heat release and increase the retention of internal and solar gains [35], [36]. Enabling night ventilation and shading would be expected to mitigate this summer effect while preserving winter savings.

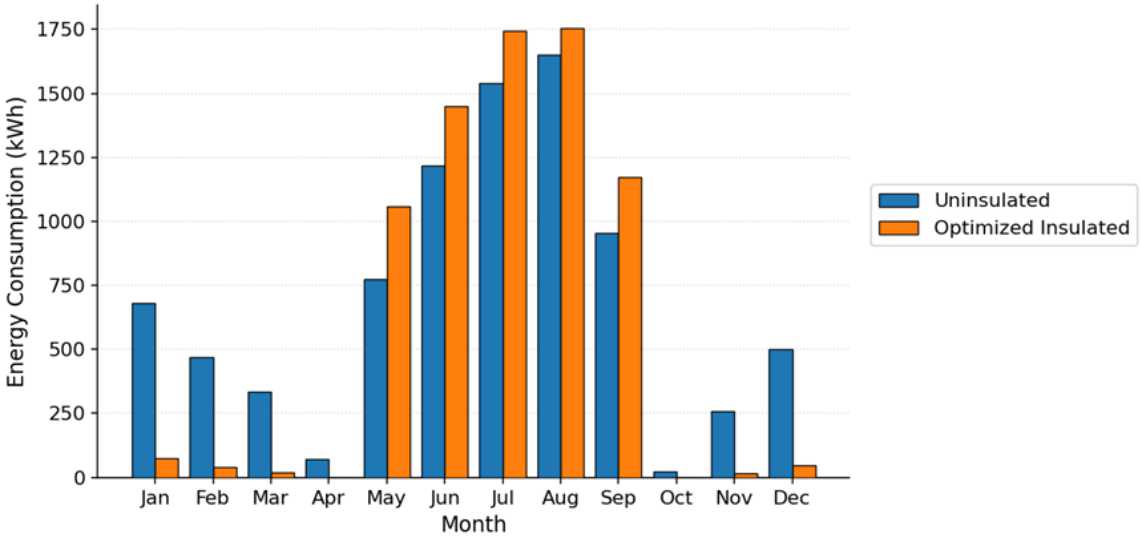

Figure 6. Monthly Total HVAC Electricity Consumption Uninsulated and Optimized Insulated

The annual hourly electricity-demand profile obtained from the selected envelope configuration is used as the input load time series for the PV – battery optimisation model described in the Method section.

Renewable Energy System Optimization

Following envelope optimization, the MILP model was applied using the optimized building load profile to identify optimal sizing and operational strategies for a hybrid PV-battery storage system **Figure 7**.

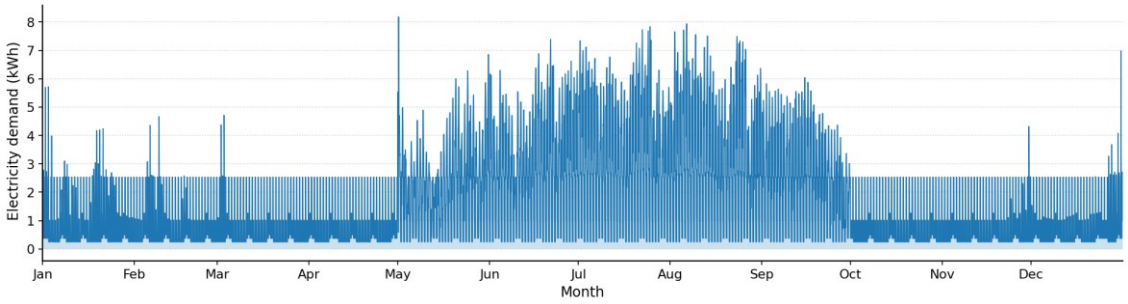

Figure 7. Hourly Electricity Demand Throughout the Year

Optimal system sizing: the mixed-integer linear programme co-sizes capacities with hourly dispatch. **Table 4** reports the cost-optimal designs for S1–S3 and shows a consistent hierarchy aligned with the incremental flexibility introduced across scenarios. Moving from S1 to S2 yields the dominant service improvement because storage relaxes the coincidence constraint between PV generation and demand: *SSR* increases by +0.302, while annual total cost decreases by 18.6% and *LCOE* decreases by 18.1%. Moving from S2 to S3 delivers a smaller additional *SSR* gain but a clear economic improvement through surplus value recovery: annual total cost decreases by 9.8% and *LCOE* decreases by 9.6%. This ranking reflects the underlying mechanisms: storage increases on-site supply by shifting midday PV into evening demand, whereas paid export primarily reduces net cost by monetising residual PV surplus that cannot be absorbed by the load or battery.

Table 4. Optimal PV–BESS sizing and KPIs by scenario

Scenario	PV capacity (kW)	BESS capacity (kWh)	SSR	Annual total cost (USD/y)	LCOE (USD/kWh)
S1	8.00	0.00	0.464	1839.13	0.127
S2	10.4	11.8	0.766	1497.17	0.104
S3	10.9	13.5	0.813	1350.92	0.094

A complementary annual energy-balance interpretation reinforces this comparison. For the same annual load (14.45 MWh), the S1 optimum supplies 6.70 MWh/y directly to the load, with the remainder (7.74 MWh/y) purchased from the grid. In S2, storage creates a second on-site supply pathway: PV supplies 7.09 MWh/y directly and the battery contributes 3.98 MWh/y, reducing grid purchases to 3.38 MWh/y. In S3, the same time-shifting channel is strengthened (battery-to-load rises to 4.51 MWh/y) and grid purchases fall further to 2.70 MWh/y, while an additional outlet appears in the form of remunerated exports (2.98 MWh/y). These flow shifts explain why the major SSR increase occurs between S1 and S2, whereas the additional cost reduction in S3 is achieved mainly through monetising surplus rather than through a proportional expansion of on-site supply.

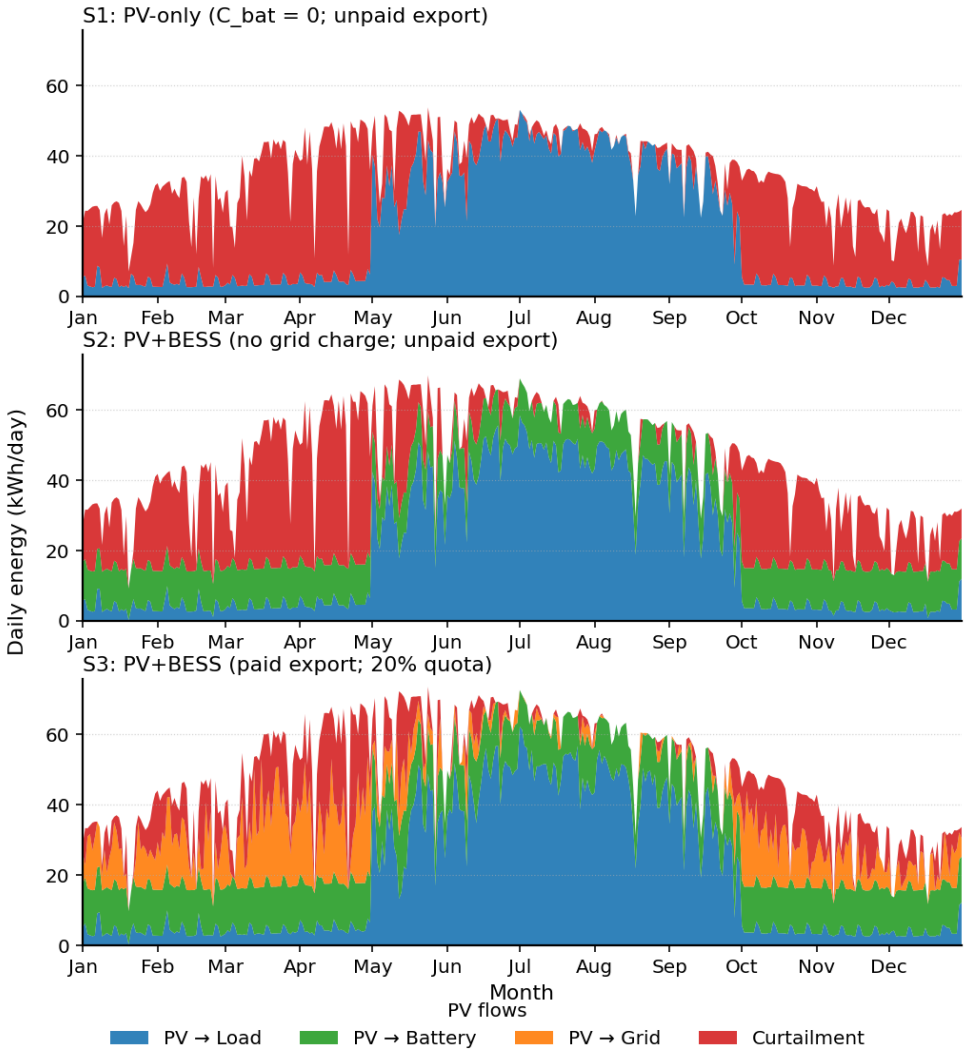

Figure 8. Daily PV flow components: load, battery, export, curtailment (S1–S3)

The fractional distribution of PV energy destinations **Figure 8** provides a mechanism-level explanation for the diminishing returns observed as capacities scale. In S1, the productive sink is strictly limited to contemporaneous demand, leading to a rapid saturation of on-site supply and a corresponding surge in curtailment as capacity increases. S2 introduces the battery as a secondary sink, which effectively captures a significant share of midday excess; however, this time-shifting channel remains bandwidth-limited, and residual surplus re-emerges once the storage absorption capacity is reached. S3 demonstrates the highest resource utilization by incorporating grid export as a systematic outlet for energy that cannot be absorbed by the load or battery. This routing logic illustrates that as the system expands, it progressively shifts from converting incremental PV into avoided grid purchases toward managing increasing volumes of surplus, which inherently drives the observed concavity in *SSR* gains.

The temporal manifestation of these routing differences is captured in the year-round daily operational profiles **Figure 9**, which highlight when scenario constraints matter most. S1 is characterized by a "self-sufficiency ceiling" during high-production months, where massive midday surpluses coexist with persistent nocturnal grid reliance due to the lack of intertemporal flexibility. S2 fundamentally restructures this relationship, substituting battery discharge for a large share of non-solar demand and substantially reducing grid interaction during the high-insolation mid-year period. S3 preserves this time-shifting contribution while improving net economics through export monetization; notably, the load-supply structure of S3 remains largely similar to S2, confirming that the principal distinction between these two

scenarios is expressed more strongly in cost-based indicators (Total Cost and *LCOE*) than in physical service delivery. Collectively, these operational dynamics establish a coherent causal chain where scenario-specific constraints determine the PV routing, which in turn governs the achievable SSR and the ultimate economic performance of the system.

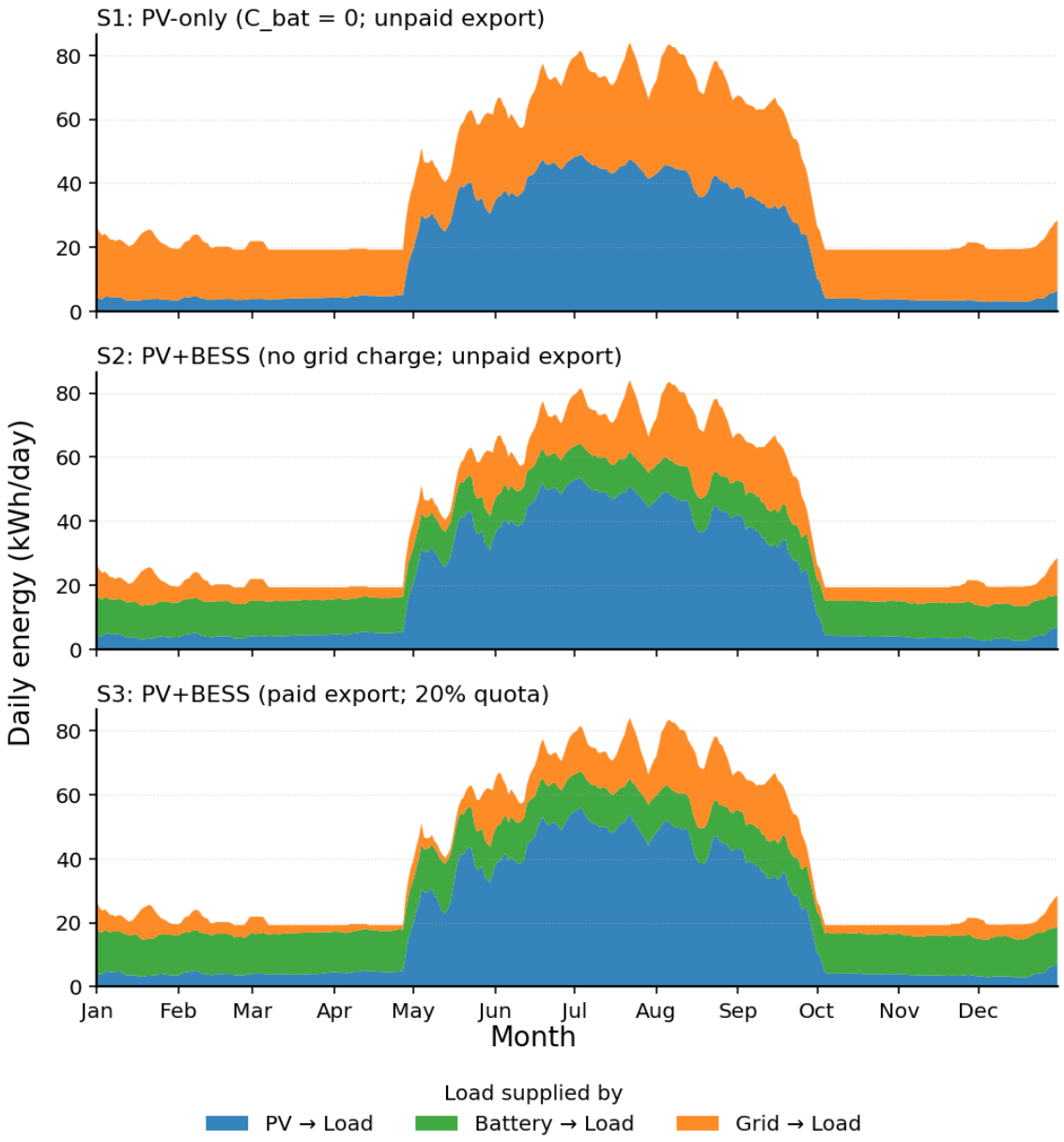

Figure 9. Daily load supply mix: PV, battery, grid (S1–S3)

The cost-optimal photovoltaic and battery capacities obtained in this study (photovoltaic 10.4 – 10.9 kW; battery 11.8 – 13.5 kWh) are larger than the photovoltaic capacities reported for net-zero annual balance in a prototypical Moroccan single-family dwelling with a 90 m² roof, where required photovoltaic capacity ranges from 1.92 to 6.00 kW across six climate zones[11]. This difference is consistent with the higher electrified annual demand represented in this study and with a cost-minimisation formulation that does not impose a net-zero annual constraint. In terms of storage magnitude, the battery energy capacity is comparable to the off-grid residential configuration evaluated for Fez by Mekila Mbayam and Bounahmidi [37], which combines 3.6 kW of installed photovoltaic capacity with approximately 11.9 kWh of lithium iron phosphate battery storage, and this value falls within the optimal battery range identified in this study. By contrast, their photovoltaic capacity is substantially smaller than the

range obtained in this study, reflecting differences in modelling objectives and constraints: their sizing is driven by meeting an annual energy-balance target with simulation-based design choices, whereas the present work endogenizes photovoltaic capacity through dispatch-constrained, full-year mixed-integer optimisation under time-of-use pricing and explicit operational limits, which can justify larger photovoltaic installations until marginal value is eroded by surplus and system constraints.

To assess robustness and marginal returns beyond the cost-optimal designs (step 0), a coordinated capacity-expansion sweep is performed.

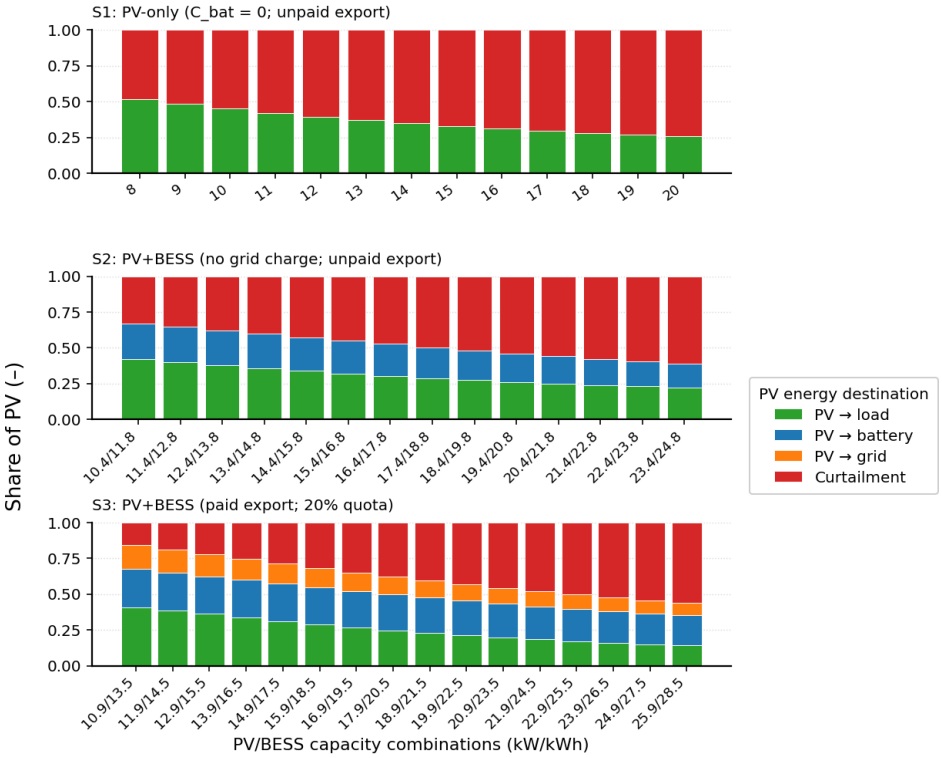

Figure 10. Sensitivity summary of PV energy destinations across incremental PV and BESS capacity combinations for Scenarios S1, S2, and S3

Figure 10 provides a mechanism-level explanation for the diminishing returns and clarifies cross-scenario contrasts. At the cost optima (step 0), annual PV generation increases from 12.92 MWh/y (S1) to 16.79 MWh/y (S2) and 17.68 MWh/y (S3). However, additional PV does not translate one-for-one into useful on-site supply because the binding limitation is temporal mismatch rather than annual resource availability. In S1, the productive sink is restricted to contemporaneous demand, so surplus emerges once daytime demand is saturated (approximately 6.22 MWh/y at the optimum, computed as PV generation minus PV-to-load). In S2, storage introduces a second sink: PV-to-battery reaches 4.15 MWh/y at the optimum and reappears as 3.98 MWh/y delivered from the battery to the load (net of charge/discharge losses), which increases on-site supply; nevertheless, the time-shifting channel remains bandwidth-limited and residual surplus persists (approximately 5.56 MWh/y at the optimum, computed as PV generation minus PV-to-load and PV-to-battery). In S3, export provides an additional outlet once the battery absorption saturates: PV-to-grid reaches 2.98 MWh/y at the optimum, reducing residual surplus to approximately 2.77 MWh/y and improving net economics without requiring a proportional increase in on-site self-supply. Across the sweep, these scenario-specific sinks explain the observed concavity: as capacities increase, the system progressively shifts from converting incremental PV into avoided grid purchases toward managing increasing volumes of surplus via export (S3) and/or residual surplus (all scenarios), which inherently yields diminishing *SSR* gains.

Table 5. Sensitivity summary of technical and economic performance indicators across PV and battery sizing increments for Scenarios S1–S3

Scenario	Step	PV (kW)	Battery (kWh)	Annual total cost (USD/y)	Savings vs baseline (USD/y)	SSR (–)	LCOE (USD/kWh)
S1	0	8.0	0.0	1,839.13	378.90	0.464	0.127
	3	11.0	0.0	1,893.92	324.11	0.519	0.131
	6	14.0	0.0	1,996.08	221.95	0.545	0.138
	9	17.0	0.0	2,115.06	102.98	0.560	0.146
	11	19.0	0	2,198.12	19.91	0.569	0.152
S2	0	10.4	11.8	1,497.17	720.86	0.766	0.104
	3	13.4	14.8	1,559.28	658.75	0.882	0.108
	6	16.4	17.8	1,700.94	517.08	0.951	0.118
	9	19.4	20.8	1,901.03	317.00	0.985	0.132
	12	22.4	23.8	2,137.62	80.41	0.996	0.148
S3	0	10.9	13.5	1,350.92	867.11	0.813	0.094
	4	14.9	17.5	1,461.01	757.01	0.939	0.101
	8	18.9	21.5	1,714.81	503.21	0.987	0.119
	12	22.9	25.5	2,034.78	183.25	0.998	0.141
	14	24.9	27.5	2,202.77	15.26	0.999	0.153

Table 5 quantifies the cross-scenario trade-offs implied by **Figure 8** and highlights where marginal returns begin to collapse. In S1, PV upsizing produces progressively smaller service gains while economic performance weakens: increasing PV from 8 to 17 kW raises *SSR* by only +0.096, while annual total cost increases by 276 USD/y and LCOE rises by +0.019 USD/kWh; savings compress sharply over the same range, indicating that additional PV increasingly converts into low-value surplus rather than avoided purchases. In S2, early co-upsizing yields large *SSR* gains at moderate cost for example, from step 0 to step 3, *SSR* increases by +0.116 for a cost increase of 62 USD/y whereas later steps exhibit clear saturation: from step 9 to step 12, *SSR* increases by only +0.011 while annual total cost increases by 237 USD/y and *LCOE* rises from 0.132 to 0.148 USD/kWh. In S3, paid export shifts the economic frontier outward at high *SSR* levels for example, step 0 to step 4 increases *SSR* by +0.126 with 110 USD/y additional cost and a small *LCOE* change (0.094 to 0.101 USD/kWh) but at larger sizes the marginal service gain collapses (step 12 to step 14 adds only +0.001 *SSR*) and savings approach breakeven (15 USD/y at step 14), signalling that further upsizing is dominated by surplus management rather than additional useful on-site supply. Overall, *SSR* improvements are concave in all scenarios, and the economic indicators track this saturation: once *SSR* is high, additional capacity yields limited avoided purchases, so annual total cost and *LCOE* increase and savings compress toward zero.

Policy sensitivity analysis: feed-in tariff and export allowance. **Figure 11** summarises how the cost-optimal PV–battery design responds to the feed-in tariff (P_{exp}) and the export allowance (S_{exp}). Two thresholds are apparent. First, curtailment is rapidly eliminated as S_{exp} increases: at P_{exp} = 0.2 and S_{exp} = 20%, 2,767 kWh of 16,855 kWh PV generation is curtailed (16.4%), whereas curtailment reaches 0.0% for multiple cases from export capacity share in range 35%–40%. Second, a regime shift occurs near S_{exp} = 70%, beyond which design and operating indicators stabilise and the marginal gains in savings progressively saturate.

Net savings relative to the baseline increase monotonically with export capacity share and with P_{exp} **Figure 11a**. At high P_{exp}, the savings response saturates beyond S_{exp}= 0.70; at P_{exp} = 0.8, savings increase from approximately 920 USD/y (S_{exp} = 0.20) to 2,075 USD/y (S_{exp}= 0.70), while export revenue plateaus at 2,268.55 USD/y for $S_{\text{exp}}\geq$ 0.70. Consistently, PV capacity increases with export_cap_share and reaches a stable plateau by export capacity share in range 0.65–0.70 in the high-P_{exp} cases **Figure 11c**.

Battery sizing exhibits a discontinuous adjustment at the regime boundary. At P_{exp} = 0.8, battery capacity decreases from 16.02 kWh at S_{exp} = 0.65 to 10.53 kWh at S_{exp} = 0.70, coincident with PV saturation at 25 kW. This shift is mirrored in operating shares: PV -to-battery share decreases from 21.6% at S_{exp} = 0.65 to 9.2% at S_{exp} = 0.70 (P_{exp} = 0.8), while PV-to-grid share approaches its upper plateau (70%) for $S_{\text{exp}} \geq$ 0.70. The reduced storage contribution increases grid purchases despite higher export monetisation: at P_{exp} = 0.8, annual grid cost drops to 82.53 USD/y at S_{exp} = 0.65 but rises to 312.61 USD/y at S_{exp} = 0.70 and remains stable thereafter **Figure 11b**.

The post-0.70 behaviour reflects a structural reallocation in the optimal investment and dispatch. Once the permitted export fraction is sufficiently high, the export-share constraint no longer limits the optimum, and remunerated exports provide a strong marginal value for additional photovoltaic generation. The optimiser therefore prioritises PV expansion until it reaches its saturation level, while battery energy capacity is reduced because the incremental benefit of time-shifting surplus PV into evening demand becomes smaller than the benefit of exporting surplus PV directly at the prevailing P_{exp}. This battery step-down reduces the system's ability to cover non-solar hours with stored PV, which explains the discontinuous increase in grid purchases. Simultaneously, because PV export revenue already operates near its plateau, further increases in export capacity share yield limited additional value, producing the observed flattening of the savings curve. In effect, S_{exp} = 0.70 marks the transition to an export-oriented optimum characterised by PV capacity saturation, lower storage dependence, and diminishing marginal gains in annual savings.

Overall, the results show that envelope optimisation materially reduces the space-conditioning electricity demand and establishes the hourly load basis for system sizing. The cost-optimal photovoltaic-only case reaches moderate self-supply, whereas adding battery storage produces the largest increase in self-supply by shifting midday generation to evening demand. Introducing paid export further improves the economic outcome mainly through surplus value recovery, with a smaller additional increase in self-supply. Capacity-expansion sweeps confirm diminishing marginal returns: beyond the optima, additional capacity increasingly converts into surplus rather than avoided grid purchases. Finally, the policy sensitivity indicates that export remuneration and export allowance can materially shift the optimal photovoltaic – battery balance, highlighting the dependence of sizing outcomes on regulatory conditions.

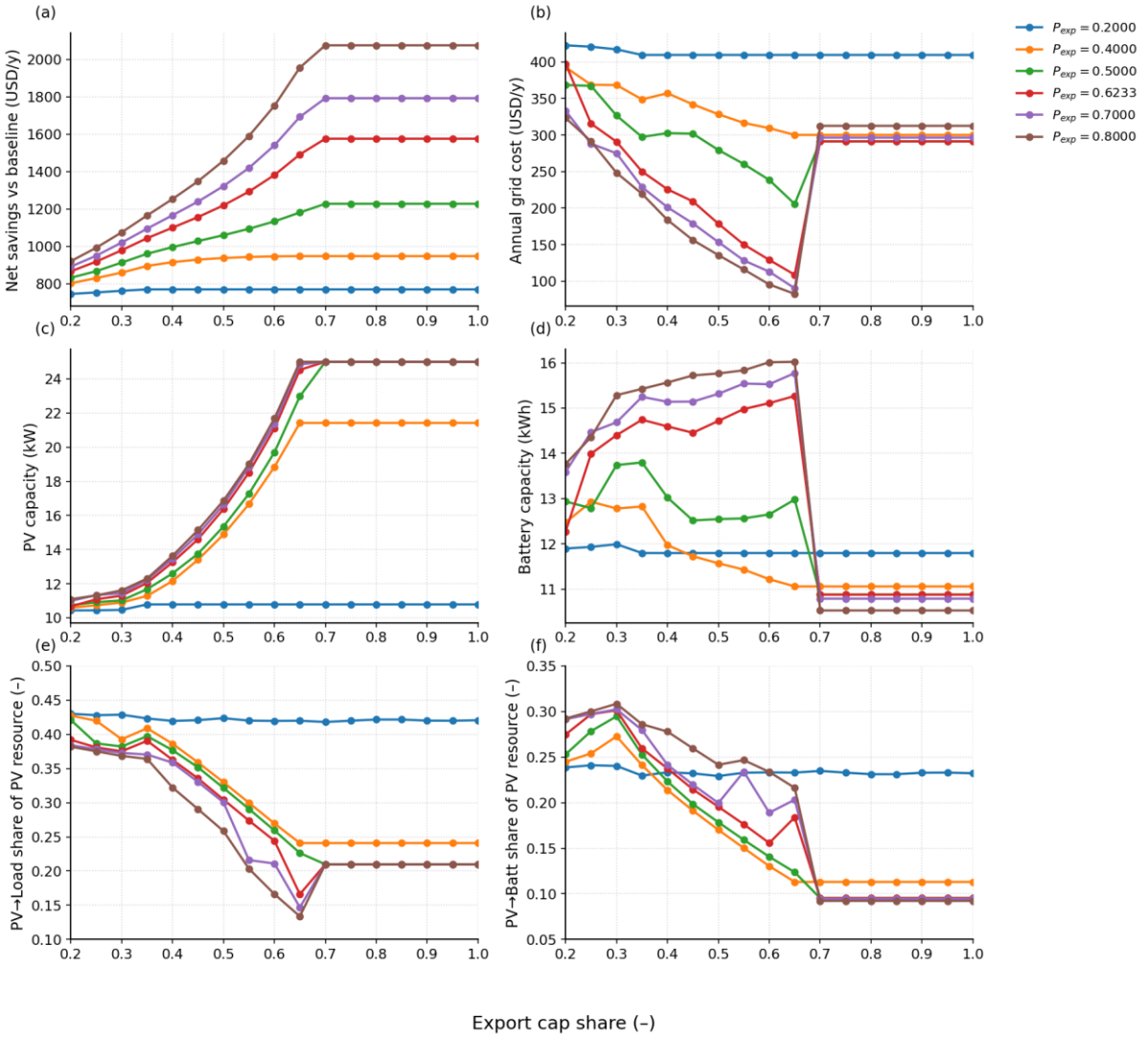

Figure 11. Sensitivity of the cost-optimal photovoltaic–battery design to export allowance and feed-in tariff: (a) Net savings vs baseline; (b) Annual grid cost.; (c) Photovoltaic capacity; (d) Battery energy capacity; (e) Photovoltaic-to-load share of photovoltaic generation; (f) Photovoltaic-to-battery share of photovoltaic generation

CONCLUSION

This study provides a policy-aware framework for reducing electricity use and emissions in Moroccan dwellings by coupling envelope demand reduction with cost-optimal rooftop photovoltaic generation and battery storage. Envelope optimisation via a multi-objective genetic algorithm reduces annual space-conditioning electricity demand by 26.9% relative to the baseline, after which a mixed-integer linear programme co-sizes photovoltaic and battery capacities and optimises hourly dispatch under the National Office of Electricity and Drinking Water time-of-use tariff structure, the no grid-to-battery charging rule, and a capped paid-export option.

The results indicate that demand reduction is a prerequisite for effective renewable-system sizing because it lowers and reshapes the hourly load profile. Under zero export remuneration, adding battery storage yields the largest increase in self-supply by shifting midday photovoltaic generation toward evening demand, although gains saturate as storage energy capacity and power limits become binding. Export conditions emerge as the dominant economic lever when remuneration is introduced: policy sensitivity shows a distinct regime transition once the permitted export allowance approaches 70%, after which photovoltaic capacity and operating indicators become comparatively stable while the cost-optimal battery

capacity drops discontinuously. This behaviour reflects a shift in value from time-shifting toward direct sale of surplus electricity to the grid, and it explains both the stabilisation of the design and the reduced marginal benefit of further export-allowance increases once export revenues approach a plateau.

The findings support an "efficiency-first, then right-size" strategy. For the Oujda case study, key performance indicators are most favourable near the identified sizing region (about 10 kW photovoltaic and about 12 kWh battery energy capacity), whereas further upsizing delivers diminishing self-supply gains while increasing annual total cost and the levelized cost of electricity. From a regulatory perspective, finalising a bankable export remuneration scheme and clarifying export allowances would shift the economic frontier more strongly than marginal adjustments elsewhere, because these terms determine whether surplus photovoltaic generation is curtailed, stored, or sold to the grid.

Several limitations should be noted in line with the scope and policy context of the analysis. The results are derived from a single representative dwelling in Oujda and therefore quantify system behaviour under one climatic setting and one load profile, rather than providing a nationally representative estimate. In addition, the economic conclusions are policy-contingent: they reflect the tariff structure, export remuneration assumptions, and export-allowance rules assessed, which remain subject to regulatory clarification and future adjustment. Accordingly, the reported optimal sizing and the identified export-driven regime shift should be interpreted as indicative of how design incentives respond to the prevailing regulatory framework, rather than as fixed values that would apply under alternative market conditions or revised grid-integration rules. Nevertheless, the modelling–optimisation workflow is transferable: applying it to other regions requires substituting the relevant climate files (weather data) and regional load profiles, and re-running the sizing optimisation under the local tariff/export scheme and grid-integration rules. Thus, while the numerical optima are case-specific, the approach provides a decision framework that can be adapted to other climates and policy regimes.

Future work should extend the framework to additional Moroccan building archetypes and climates, incorporate multi-year and stochastic inputs, represent flexible loads and demand response, integrate grid-aware constraints, and evaluate robustness to tariff and policy uncertainty (including alternative export remuneration levels and export-allowance rules). Within these bounds, the proposed genetic-algorithm-to-mixed-integer-linear-programming workflow provides a reproducible approach for producing physically credible designs that link envelope efficiency, photovoltaic generation, and battery storage decisions to Morocco's evolving tariff and export policy environment.

ACKNOWLEDGMENTS

The paper is prepared within the framework of the EMERGE project, Call for proposals: HORIZON-CL5-2022-D3-02. Project number: 101118278. Type of action: Research and innovation actions HORIZON, 2023.

NOMENCLATURE

Symbols

$big - M$	tight big-M gating constant	[kW]
C_{bat}	battery energy capacity	[kWh]
C_{rate}	battery c-rate (power per energy)	[kW/kWh]
$c^{\mathrm{t}}_{\mathrm{pv,OM}}$	PV variable operations and maintenance cost	[USD/kWh]
$c_{\mathrm{bat,E}}$	battery energy CAPEX coefficient	[USD/kWh]

$c_{\mathrm{bat,P}}$	battery power CAPEX coefficient	[USD/kW]
c_{LL}	lost-load penalty	[USD/kWh]
c_{pv}	photovoltaic capital cost	[USD/kW]
CRF	capital recovery factor	[-]
$E^t_{\mathrm{b}\to\mathrm{l}}$	battery discharge to load at hour *t*	[kWh]
$E^t_{\mathrm{g}\to\mathrm{b}}$	grid energy to battery at hour *t*	[kWh]
$E^t_{\mathrm{g}\to\mathrm{l}}$	grid energy to load at hour *t*	[kWh]
$E^t_{\mathrm{p}\to\mathrm{b}}$	PV energy to battery at hour *t*	[kWh]
$E^t_{\mathrm{p}\to\mathrm{g}}$	PV energy exported to gride at hour *t*	[kWh]
$E^t_{\mathrm{p}\to\mathrm{l}}$	PV energy to load at hour *t*	[kWh]
EUI	energy use intensity	[kWh·m^{-2}·y^{-1}]
L^t	electric load at hour *t*	[kWh]
LL^t	lost load (unserved energy) at hour *t*	[kWh]
$LCOE$	levelized cost of electricity	[USD/kWh]
p^t	grid import price (TOU)	[USD/kWh]
P_{exp}	export price (when applicable)	[USD/kWh]
P_{pv}	installed photovoltaic power	[kW]
PV^t	specific pv yield (EHDO)	[kWh/kW]
PV^t_{resource}	PV energy available	[kWh]
S_{exp}	export capacity share	[-]
SOC^t	state of charge at end of hour *t*	[kWh]
SOC_{min}	minimum admissible state of charge	[kWh]
SOC^0	initial state-of-charge fraction	[-]
SSR	self-supply ratio	[-]
U	thermal transmittance	[Wm^{-2}K^{-1}]
R	thermal resistance	[m²kW^{-1}]
$y^t_{\mathrm{chg,grid}}$	grid-charging mode binary (0/1)	[-]
$y^t_{\mathrm{chg,pv}}$	PV-charging mode binary (0/1)	[-]
y^t_{dis}	discharging mode binary (0/1)	[-]

Greek letters

η_{chg}	charge efficiency
η_{dis}	discharge efficiency

Subscripts and superscripts

b	battery (flow node)
bat	battery (capacity parameter)
chg	charging mode

dis	discharging mode
exp	export
g	grid (flow node)
l	load (flow node)
min	minimum
p	photovoltaic (flow node)
pv	photovoltaic
rt	round-trip (efficiency)
*	optimal value
0, 8760	initial, end-of-year value

Abbreviations

AC	Alternating Current
ANRE	National Electricity Regulatory Authority
BESS	Battery Energy Storage System
BIM	Building Information Modelling
CAPEX	Capital Expenditure
COP	Coefficient of Performance
CRF	Capital Recovery Factor
C-rate	Battery Charge/Discharge Rate
DC	Direct Current
DHW	Domestic Hot Water
EEM	Energy Efficiency Measure
EER	Energy Efficiency Ratio
EHDO	Energy Hub Design Optimizer (open-source tool)
EMS	Energy Management System
EPW	EnergyPlus Weather (file format)
EUI	Energy Use Intensity
EV	Electric Vehicle
GA	Genetic Algorithm
GenOpt	Generic Optimisation Tool (for TRNSYS)
GHI	Global Horizontal Irradiance
HVAC	Heating, Ventilation and Air Conditioning
IBPSA	International Building Performance Simulation Association
ICF	Insulated Concrete Form
KPI	Key Performance Indicator
LCOE	Levelized Cost of Electricity
LEEM	Laboratory of Electrical Engineering and Maintenance
Low-E	Low-Emissivity
MAD	Moroccan Dirham
MILP	Mixed-Integer Linear Programming
MPC	Model Predictive Control
NH	Normal Hours
NSGA-II	Nondominated Sorting Genetic Algorithm II
O&M	Operations and Maintenance
ONEE	Office National de l'Électricité et de l'Eau Potable
PH	Peak Hours
PV	Photovoltaic

SIP	Structural Insulated Panel
S1 / S2 / S3	Scenario Labels
SSR	Self-Supply Ratio
TOU	Time-of-Use
TRNSYS	Transient System Simulation Tool

REFERENCES

1. Agence Nationale de Régulation de l'Électricité (ANRE), Annual Report 2024, Agence Nationale de Régulation de l'Electricité, Rabat, Morocco, Dec. 2025, https://anre.ma/en/publications/rapports-annuels/, [Accessed: Mar. 14, 2026]
2. Moroccan Agency for Energy Efficiency (AMEE), Thermal Building Regulations in Morocco (in French, Règlement thermique de construction au Maroc), Rabat, Morocco, Dec. 2015, https://amee.ma/sites/default/files/inline-files/Reglement_thermique_de_construction_au_Maroc.pdf, [Accessed: Dec. 17, 2025]
3. H. El Hafdaoui, A. Khallaayoun, and S. Al-Majeed, Renewable energies in Morocco: A comprehensive review and analysis of current status, policy framework, and prospective potential, *Energy Conversion and Management: X*, Vol. 26, 2025, https://doi.org/10.1016/j.ecmx.2025.100967.
4. W. Arfaoui, M. Karmoun, K. Azzakhnini, M. L. Elhafyani, S. Zouggar, H. Zahboune, T. Ouchbel, A. A. Becerra, and N. Matak, Assessment of the Hosting Capacity of the Moroccan Electricity Grid for the Integration of Renewable Energies, *Journal of Sustainable Development of Energy, Water and Environment Systems*, Vol. 14, No. 1, 113064, 2025, https://doi.org/10.13044/j.sdewes.d13.0643.
5. National Office of Electricity and Drinking Water (ONEE), Official website, http://www.one.org.ma/, [Accessed: Dec. 17, 2025].
6. C. Lorenz, D. R. Bayer, M. Pruckner, T. Staake, and K. Hopf, Do dynamic electricity tariffs change the gains of residential PV-battery systems? A simulation-based evaluation using data from 448 households, *Energy Policy*, Vol. 209, 2026, https://doi.org/10.1016/j.enpol.2025.114952.
7. G. U. Magni, D. Bricca, and S. Familiari, Economic Incentives for Renewable Energy Communities: a Scenario Analysis in the Transition Process Between the Experimental and Definitive Italian Policy Framework, *Journal of Sustainable Development of Energy, Water and Environment Systems*, Vol. 13, No. 2, 2025, https://doi.org/10.13044/j.sdewes.d13.0589.
8. Agence Nationale de Régulation de lÉlectricité (ANRE), Decision No. 04/26 setting the tariff for surplus electrical energy produced under Laws No. 40-19 and No. 82-21 (in French, Décision n°04/26 fixant le tarif de lexcédent de lénergie électrique produite dans le cadre des lois n°40-19 et n°82-21), Agence Nationale de Régulation de lElectricité, Rabat, Morocco, Feb. 2026, https://anre.ma/publications/, [Accessed: Mar. 14, 2026].
9. C. Citadini de Oliveira, I. Catão Martins Vaz, and E. Ghisi, Retrofit strategies to improve energy efficiency in buildings: An integrative review, *Energy Build.*, Vol. 321, p. 114624, 2024, https://doi.org/10.1016/j.enbuild.2024.114624.
10. N. Abdou, Y. EL Mghouchi, S. Hamdaoui, N. EL Asri, and M. Mouqallid, Multi-objective optimization of passive energy efficiency measures for net-zero energy building in Morocco, *Build. Environ.*, Vol. 204, 2021, https://doi.org/10.1016/j.buildenv.2021.108141.
11. K. Boumlik, R. Belarbi, M. Ahachad, M. Mahdaoui, H. Radoine, and M. Krarti, Design Optimization of Energy-Efficient Residential Buildings in Morocco, *Buildings*, Vol. 14, No. 12, 2024, https://doi.org/10.3390/buildings14123915.
12. F. Zahra Benaddi, L. Boukhattem, and P. Cesar Tabares-Velasco, Multi-objective optimization of building envelope components based on economic, environmental, and

thermal comfort criteria, *Energy Build.*, Vol. 305, 113909, 2024, https://doi.org/10.1016/J.ENBUILD.2024.113909.

13. K. Alexakis, V. Benekis, P. Kokkinakos, and D. Askounis, Genetic algorithm-based multi-objective optimisation for energy-efficient building retrofitting: A systematic review, *Energy Build.*, Vol. 328, 2025, https://doi.org/10.1016/j.enbuild.2024.115216.
14. D. Jakus, J. Novaković, J. Vasilj, and D. Jolevski, Optimal Residential Battery Storage Sizing Under ToU Tariffs and Dynamic Electricity Pricing, *Energies (Basel).*, Vol. 18, No. 9, 2025, https://doi.org/10.3390/en18092391.
15. A. Kesküla, K. Grjaznov, T. Sepp, and A. Allik, Optimal Sizing of Residential PV and Battery Systems Under Grid Export Constraints: An Estonian Case Study, *Energies (Basel).*, Vol. 18, No. 16, 2025, https://doi.org/10.3390/en18164405.
16. J. Yu, Y. Zhang, Z. Yan, L. Chen, and W. Fu, A Multi-Objective Optimized Approach to Photovoltaic-Battery Systems Constrained by Transformer Capacity for Existing Buildings, *Energies (Basel).*, Vol. 18, No. 13, 2025, https://doi.org/10.3390/en18133339.
17. Y. Hou, Q. Yuan, X. Wang, H. Chang, C. Wei, D. Zhang, Y. Dong, Y. Yang, and J. Zhang, Parameter Design of a Photovoltaic Storage Battery Integrated System for Detached Houses Based on Nondominated Sorting Genetic Algorithm-II, *Buildings*, Vol. 14, No. 6, 2024, https://doi.org/10.3390/buildings14061834.
18. M. Rezaeimozafar, M. Khoshkar, J. Ramezani, S. Babaie, and A. Azari, A stochastic method for behind-the-meter PV-battery energy storage systems sizing with degradation minimization by limiting battery cycling, *J. Energy Storage*, Vol. 86, 2024, https://doi.org/10.1016/j.est.2024.111199.
19. T. Dias de Lima, P. Faria, and Z. Vale, Optimizing home energy management systems: A mixed integer linear programming model considering battery cycle degradation, *Energy Build.*, Vol. 329, 2025, https://doi.org/10.1016/j.enbuild.2024.115251.
20. K. Boumlik, Z. Romani, H. Radoine, H. Mastouri, and M. Ahachad, Overview of the existing residential construction practices in Morocco: A building energy simulation and thermal comfort analysis, *Journal of Building Engineering*, Vol. 112, p. 113783, 2025, https://doi.org/10.1016/j.jobe.2025.113783.
21. S. Gheouany, H. Ouadi, and S. El Bakali, Optimal active and reactive energy management for a smart microgrid system under the Moroccan grid pricing code, *Energy*, Vol. 306, 2024, https://doi.org/10.1016/j.energy.2024.132462.
22. U. Mumtahina, S. Alahakoon, and P. Wolfs, A Day-Ahead Optimal Battery Scheduling Considering the Grid Stability of Distribution Feeders, *Energies (Basel).*, Vol. 18, No. 5, 2025, https://doi.org/10.3390/en18051067.
23. N. Weerasinghe Mudiyanselage, A. Aziz, B. Al-Hanahi, and I. Ahmad, Cost-Optimized Energy Management for Urban Multi-Story Residential Buildings with Community Energy Sharing and Flexible EV Charging, *Sustainability (Switzerland)*, Vol. 17, No. 21, 2025, https://doi.org/10.3390/su17219717.
24. M. Pasqui, F. Gerini, M. Jacobs, C. Carcasci, and M. Paolone, Self-dispatching a renewable energy community by means of battery energy storage systems, *J. Energy Storage*, Vol. 114, 2025, https://doi.org/10.1016/j.est.2025.115837.
25. K. Z. Dadjiogou, A. S. A. Ajavon, and Y. Bokovi, Energy Flow Management in a Smart Microgrid Based on Photovoltaic Energy Supplying Multiple Loads, *Journal of Sustainable Development of Energy, Water and Environment Systems*, Vol. 12, No. 1, 2024, https://doi.org/10.13044/j.sdewes.d11.0473.
26. I. Costa-Carrapiço, R. Raslan, and J. N. González, A systematic review of genetic algorithm-based multi-objective optimisation for building retrofitting strategies towards energy efficiency, *Energy Build.*, Vol. 210, 109690, 2020, https://doi.org/10.1016/J.ENBUILD.2019.109690.

27. P. S. Georgilakis and N. D. Hatziargyriou, A review of power distribution planning in the modern power systems era: Models, methods and future research, *Electric Power Systems Research*, Vol. 121, pp 89–100, 2015, https://doi.org/10.1016/j.epsr.2014.12.010.
28. G. Stunjek and G. Krajacic, Optimisation of desalination-based water system with integrated renewable energy and storage, *Desalination*, Vol. 600, 118474, 2025, https://doi.org/10.1016/j.desal.2025.118474.
29. P. Ineichen, Comparison of eight clear sky broadband models against 16 independent data banks, *Solar Energy*, Vol. 80, No. 4, pp 468–478, 2006, https://doi.org/10.1016/j.solener.2005.04.018.
30. M. Charai, M. Boutouil, and N. Zemmouri, Bioclimatic analysis and thermal comfort assessment of residential buildings in Oujda, Morocco, *Int. J. Sustain. Built Environ.*, Vol. 8, No. 2, 2019, https://doi.org/10.1109/IRSEC48032.2019.9078176.
31. M. Maaouane, M. Chennaif, S. Zouggar, G. Krajacic, S. Amrani, and H. Zahboune, Cost-effective design of energy efficiency measures in the building sector in North Africa using multi-objective optimization, *Energy Build.*, Vol. 294, 113283, 2023, https://doi.org/10.1016/j.enbuild.2023.113283.
32. Z. Romani, A. Draoui, and F. Allard, Metamodeling the heating and cooling energy needs and simultaneous building envelope optimization for low energy building design in Morocco, *Energy Build.*, Vol. 102, pp 139–148, 2015, https://doi.org/10.1016/j.enbuild.2015.04.014.
33. M. Wirtz, P. Remmen, and D. Müller, EHDO: A free and open-source webtool for designing and optimizing multi-energy systems based on MILP, *Comput. Appl. Eng. Educ.*, Vol. 29, No. 5, pp 983–993, 2021, https://doi.org/10.1002/cae.22352.
34. H. Sghiouri, A. Mezrhab, M. Karkri, and H. Naji, Shading devices optimization to enhance thermal comfort and energy performance of a residential building in Morocco, *Journal of Building Engineering*, Vol. 18, pp 292–302, 2018, https://doi.org/10.1016/j.jobe.2018.03.018.
35. D. Fosas, D. A. Coley, S. Natarajan, M. Herrera, M. Fosas de Pando, and A. Ramallo-Gonzalez, Mitigation versus adaptation: Does insulating dwellings increase overheating risk?, *Build. Environ.*, Vol. 143, pp 740–759, 2018, https://doi.org/10.1016/j.buildenv.2018.07.033.
36. M. Fallah and Z. Medghalchi, Proposal of a new approach for avoiding Anti-Insulation in residential buildings by considering occupants comfort condition, *Therm. Sci. Eng. Prog.*, Vol. 20, p. 100721, 2020, https://doi.org/10.1016/j.tsep.2020.100721.
37. O. Mekila Mbayam and T. Bounahmidi, Energy optimization of a residential building for electricity, cooling, and heating: A path to Net Zero Energy, *Energy for Sustainable Development*, Vol. 85, 2025, https://doi.org/10.1016/j.esd.2025.101672.

Paper submitted: 03.10.2025
Paper revised: 16.03.2026
Paper accepted: 21.03.2026